Materials Advances

ROYAL SOCIETY OF CHEMISTRY

PAPER

View Article Online
View Journal | View Issue

Cite this: *Mater. Adv.*, 2024, 5, 306

Surfactant-assisted synthesis of zero-dimensional iron nanomaterial for cellobiose hydrolysis†

Hari Singh, *[ab] Anil Kumar Sinha,[b] Sharanmeet Kour,[a] Suneel Singh Barheyan,[d] Gaurav Goel[c] and Jibanananda Mishra[ae]

A cost-effective, magnetically separable iron nanomaterial (15 wt% Fe) was synthesized using cetyl trimethylammonium bromide (CTAB) as a template and used for the hydrolysis of cellobiose at 120 °C. The m-FeCTB catalyst is ferromagnetic, mesoporous, and crystalline with a dominant γ-Fe_2O_3 phase; it has a high surface area (30 m^2 g^{-1}) and small particle size (60 nm). The cellobiose hydrolysis achieved a glucose yield of 60% and hydromethyl furfural (HMF) yield of 40% at 6 h. This catalytic activity with a turnover frequency of 0.037 s^{-1} and selectivity for glucose and HMF was attributed to high surface area, calcination temperature (400 °C), crystallinity, metallic site, surface acidity (26 μmol g^{-1}) due to the presence of Fe^{2+}, and small particle size. The m-FeCTB catalyst showed moderate recyclability over two cycles.

Received 23rd August 2023,
Accepted 9th November 2023

DOI: 10.1039/d3ma00588g

rsc.li/materials-advances

1 Introduction

Among the renewable sources of energy, biomass accounts for ~12% of the world's total energy consumption. The conversion of biomass, the only source of carbon in nature, into value-added chemicals highlights its potential as a capable source of renewable energy and green chemicals.[1] Biomass can be obtained from several sources, including natural sources, agricultural waste, municipal waste, and industrial waste. Lignocellulosic biomass (LCB) is a biopolymer of cellulose, lignin, and hemicellulose.[2] Polysaccharides (cellulose and hemicellulose) account for ~80% of LCB and can be good source of green chemicals *via* different reaction pathways.[2] LCB is the main source for the production of biofuels such as biogasoline and biodiesel, power generation, and the production of other bio-based products. Biofuels are broadly classified into first- or second-generation biofuels. First-generation biofuels are obtained from sugar, starch, or plant oil. Conversely, second-generation biofuels are extracted from LCB.[3,4] Apart from the production of biofuels, LCB is also used to produce value-added chemicals like aldehydes, phenol, propylene glycol, succinic acid, furfural, and alcohols such as 1,3-propanediol, 1,4-butanediol, and hydromethyl furfural (HMF).[5] Cellulose, a homopolymer of glucose comprising cellobiose as the repeating unit, is linked by β-(1,4)-glycosidic bonds.[6] Cellulose comprises two components: amorphous and crystalline. Enzymes (catalysts) can conveniently digest the amorphous component rather than the crystalline component because the latter comprises microfibril chains of β-D-glucan bonded by hydrogen bonds. Conversely, hemicellulose possesses very short chains of different kinds of polysaccharides linked by glycosidic bonds. Unlike cellulose, hemicellulose easily degrades into its monosaccharide units, enabling applications in various industries.[7] Lignin comprises a multiplexed network of oxygenated polymers of *p*-propyl phenol units. In a lignocellulosic network, lignin is firmly linked with hemicellulose. Due to the intrinsic network of cellulose, hemicellulose, and lignin present in LCB, it is very difficult to convert LCB into valuable chemicals in a natural way. Therefore, a pretreatment is required to break the outermost layer of biomass and expose the cellulose and hemicellulose for hydrolysis.[8,9]

Various techniques have been employed to date for obtaining value-added chemicals from LCB, which are mainly divided into three routes, namely thermal, thermochemical, and biochemical routes.[10–14] These techniques can be categorized further into aerobic composting, anaerobic composting, steam reforming, pyrolysis, hydrothermal reaction, oxidation, reduction, gasification, open-air combustion, super adiabatic combustion, and hydrolysis. Among the various techniques employed for obtaining value-added chemicals from LCB, the hydrolysis route seems to be the most effective one due to its cost-effective nature and simple procedure with minimum steps involved, yielding bioethanol as the major product.[12–15] Hydrolysis is defined as a reaction performed in the presence of water that results in the

[a] *RIMT University, School of Basic & Applied Science (Chemistry Department), Mandi Gobindgarh, Punjab 147301, India. E-mail: harrysinghicm24@gmail.com, harisingh@rimt.ac.in*
[b] *CSIR-Indian Institute of Petroleum, Dehradun 248005, India*
[c] *School of Energy and Environment, Thapar Institute of Engineering and Technology, Patiala, 147004, India*
[d] *Department of Chemistry, Government College for Women, Udhampur 182101, J&K, India*
[e] *School of Biosciences, RIMT University, Mandi Gobindgarh, Punjab 147301, India*

† Electronic supplementary information (ESI) available. See DOI: https://doi.org/10.1039/d3ma00588g

breakdown of chemical bonds. Hydrolysis of LCB can be performed using either mineral acid, base, or catalyst or *via* enzymatic processes in homogenous phase.[16,17] Under chemical hydrolysis, LCB is treated with acids of varying concentrations, from diluted to concentrated, along with temperature variations. In homogenous mode or enzymatic processes, hydrolysis reactions have many limitations, such as undesired cascade reactions, enzyme sensitivity, and purification steps.[17–21] At high temperature using concentrated acids, hemicellulose and cellulose are hydrolyzed without lignin.[22] Conversely, at low temperature using dilute acids, hemicellulose is hydrolyzed, whereas cellulose and lignin are not hydrolyzed.[23] Alkali treatment of LCB involves the treatment of biomass with suitable alkalis. The advantage of alkali treatment is that it directly targets lignin.

A recent review on the hydrolysis of cellobiose discussed the advantages and limitations of heterogeneous catalysis for the main groups of solid acid catalysts.[24] The literature review reported the hydrolysis of oligo- or polysaccharides and model compounds (such as sucrose, maltose or cellobiose) using solid acid catalysts, zeolites, arabinoglactan, arabinoxylan,[29] and various functionalized carbons at high temperature.[23,24] The molecular mechanism of hydrolysis has been well described in the literature[10,23]; hydrolysis occurs *via* oligosaccharide adsorption using oxygen electron lone pairs or hydroxyl groups, protonation of the oxygen atom of the ether linkage, followed by the insertion of a water molecule, resulting in the cleavage of CO bond.[24] Compared to various commercially available catalysts, iron-based catalysts are more economical and effective agents for performing the process of hydrolysis. Cellulose depolymerization reactions are often complex due to extensive bonding between various monomeric units. Therefore, cellobiose might be considered a model compound for cellulose hydrolysis for the ease of product analysis. Cellobiose is a disaccharide comprising two glucose units linked by a β-1,4-glycosidic bond with molecular formula of $((C_6H_7(OH)_4O)_2O)$. Most of the reported catalytic hydrolysis of cellobiose was performed at a high temperature of ∼200 °C because, compared to other disaccharides, cellobiose is very stable against hydrolysis for its conversion into value-added chemicals.[24] The hydrolysis reaction requires a complex reaction set up, such as a fixed bed reactor or batch reactor (autoclave, Parr).[24] Recently, our group reported the template-assisted synthesis of new iron nanomaterials for latent fingerprinting.[11] This study reports the detailed cetyl trimethylammonium bromide (CTAB)-assisted synthesis and in-depth characterization of a magnetically separable iron nanomaterial and its application for the hydrolysis of cellobiose. Herein, the hydrolysis of cellobiose was performed using this nanomaterial at low temperature (120 °C) in a glass assembly, offering a simple and cost-effective process.

2 Materials and methods

2.1 Materials

Sodium hydroxide (NaOH), ethanol, and sodium borohydride ($NaBH_4$) were purchased from Loba chemicals. Ferric chloride ($FeCl_3$) and CTAB were obtained from Sigma-Aldrich. D-(+)-Cellobiose with a specific rotation of +33° to +35° used in biochemistry with a purity of >98% was purchased from Loba chemicals. Distilled water purchased from Loba Chemicals.

2.2 Method

The hydrolysis reaction was performed in a glass distillation assembly mounted on a heating mantle. The chamber was fitted with a T-shaped bend on one side for collecting the product after the completion of the reaction.

2.3 Synthesis of m-FeCTB catalyst

The coprecipitation approach was used to complete the synthesis process using CTAB as a template by modifying the method previously reported by our group.[11] As a precursor, 3 g of $FeCl_3$ and 1 g of cationic surfactant CTAB were combined with ∼500 mL of distilled water. Drop by drop, NaOH was added to this mixture and constantly stirred until the pH of the liquid reached ∼11. A pH meter was used to measure the pH. The entire reaction was conducted for 30 min at 80 °C with steady stirring. Further, hydrazine hydrate (30 mL) was added dropwise at 80 °C and stirred continuously for ∼30 min. The resulting precipitate was filtered before being dried at a maximum temperature of 80 °C in an oven. The dried material was extracted with ethanol at 80 °C to eliminate impurities before being dried in the oven once more. The dried nanomaterial was calcined at 400 °C in air for 4 h to get rid of organic impurities. The synthesized mesoporous iron nanomaterial is designated as m-FeCTB catalyst.

2.4 Catalyst characterization

The structural and microstructural characterization were performed *via* wide-angle powder X-ray diffraction (XRD, Japan Rigaku with model smart Lab) using Cu K_α radiation with λ = 1.5405 Å and a scanning speed of 5° min^{-1} in a 2θ range of 10–70°. The N_2 sorption isotherm of the m-FeCTB catalyst was measured at 77 K and 1 bar using a BelsorbMax analyzer (BEL, Japan). The specific surface area was estimated from Brunauer–Emmett–Teller (BET) model in the P/P_0 range of 0.05–0.30. The sample was pretreated at 250 °C under vacuum to remove the organic impurities. The magnetic properties were examined using a Lakeshore 7410 Series vibrating sample magnetometer (VSM). The sample was analyzed using magnetic hysteresis (MH) curve at 300 K with different magnetic fields up to 2 T. X-ray photoelectron spectroscopy (XPS) analysis was performed using an Axix Ultra DLD Kratos instrument with a monochromatic Al Kα X-ray source at 1486.6 eV. The iron nanomaterial sample was analyzed in an Ar atmosphere. The morphology of the iron nanomaterial was imaged using scanning electron microscope (SEM) with a Carl Zeiss Model Supra 55 Germany instrument at 10 kV. The sample was suspended in ethanol solution and placed on a copper grid to examine the images of multiple areas. Transmission electron microscopy (TEM) images were recorded on a Tecnai T20 operated at 200 keV. The sample was dispersed in isopropyl alcohol (IPA) by sonicating on a copper grid to obtain the images. Dynamic light

scattering (DLS) analysis was performed using a Malvern Instruments Zetasizer with a quartz cuvette at 25 °C. The surface acidity was measured by ammonia temperature-programmed desorption using a Micromeritics 2900 chemisorption instrument equipped with a thermal conductivity detector (TCD) detector. Temperature-programmed reduction (TPR) analysis was conducted using a Micromeritics TPX 2720 apparatus equipped with a TCD detector in 10% H_2/Ar mixture. Inductively coupled plasma atomic emission spectrometry (ICP-AES) analysis was used to determine the elemental composition of the nanomaterial.

The hydrolyzed products were analyzed using ultraviolet (UV) spectrophotometer (PerkinElmer UV/vis Lambda 2 spectrophotometer). The high performance liquid chromatography (HPLC) chromatograms were recorded for the hydrolyzed products and for subsequent reference. The products were analyzed *via* HPLC-mass spectrometry (Agilent 1260 Infinity HPLC system hyphenated with a 6120 single quadrupole MS detector; column temperature, 20 °C; mobile phase, 5 mM H_2SO_4 at 0.5 mL min^{-1}).

3 Results and discussion

3.1 Characterization of m-FeCTB catalyst

The crystal morphology of the synthesized iron nanomaterial was observed using TEM analysis to determine the shape and size of the nanomaterial (Fig. 1). The particle size of 45–60 nm could be seen from Fig. 1b and c; the dark parts in Fig. 1b might be due to the carbon or copper grid. The particles seemed to be interconnected and hence determination of the exact size is impossible; however, Image J software analysis of the TEM image (Fig. 1c) showed mostly nanoparticles with an average size of 45–60 nm, whereas a size of 45–120 nm (Fig. S1, ESI†) was obtained from DLS analysis.[11] The high-magnification image (Fig. 1c) showed that the particles were porous in nature, yielding distinct porosity in the catalyst material. The selected area electron diffraction (SAED) pattern with indexing (Fig. 1d) showed the high crystallinity of the nanomaterial, in agreement with the XRD results. Small particle size and porosity were required to enhance the adsorption rate of cellobiose during the hydrolysis reaction.

The SEM images (Fig. 2a–d) showed the spherical morphology of the m-FeCTB nanomaterial with a diameter of ~50 nm, which is in agreement with the TEM analysis. The SEM images showed the porous nature of the nanomaterial, as required for the hydrolysis reaction. The elemental composition was determined by ICP-AES as 26 atomic% iron and 21 atomic% mesoporous carbon.

The type IV nitrogen sorption isotherm of the iron nanomaterial was shown in Fig. 3 with a H1 hysteresis loop. The detailed description was also reported earlier by our group.[11] The average pore size was calculated to be in the range of 35 nm, and the pore volume was determined to be 0.04 $cm^3\ g^{-1}$ (Fig. 3 inset) by Barrett–Joyner–Halenda plot, indicating mesoporosity. The total surface area was calculated to be 30 $m^2\ g^{-1}$ with high precision using BET plot. The mesoporosity favors the strong adsorption of cellobiose on the surface of the catalyst with reduced activation energy and increased rate of reaction.[21,25,31]

The structural properties of the sample are ascertained from the powder X-ray diffraction (PXRD) pattern. All the XRD peaks that are evident in the spectrum (Fig. 4a) correspond to γ-Fe_2O_3, which is present in the synthesized iron nanomaterial. The synthesized nanomaterial shows characteristic peaks at 2θ values of 36°, 33°, 30°, 54°, 59°, and 63°, corresponding to the reflections from the (311), (211), (220), (422), (333), and (440) planes, respectively. The characteristic sharp and large peak at the 2θ value of 36° for the (311) plane is ascribed to the γ-Fe_2O_3. The XRD results confirm the crystalline nature of the synthesized nanomaterial. PXRD (Fig. 4b) shows the amorphous nature of the uncalcined Fe_2O_3 nanomaterial. The PXRD spectrum of the calcined Fe nanomaterial indicates the crystalline structure with characteristic sharp peaks (Fig. 4a) corresponding to γ-Fe_2O_3.

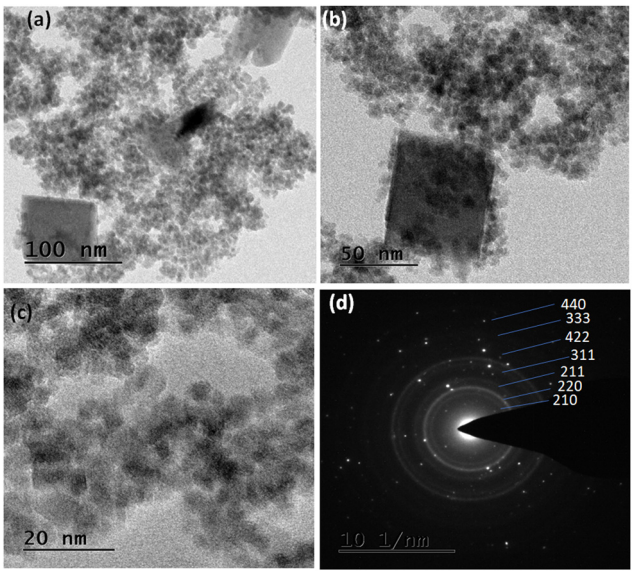

Fig. 1 (a) TEM image of Fe nanomaterials (m-FeCTB catalyst) at 200 nm, (b) 50 nm, and (c) 20 nm. (d) SAED image of Fe nanomaterials.

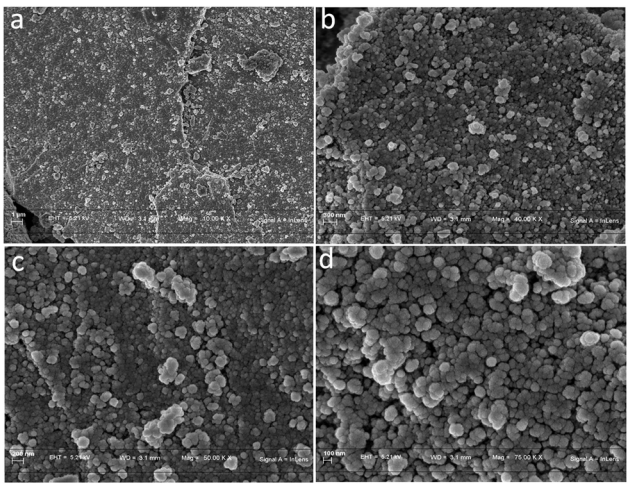

Fig. 2 (a) SEM images of m-FeCTB at 1 μm, (b) 300 nm, (c) and 200 nm, and (d) FESEM image at 100 nm.

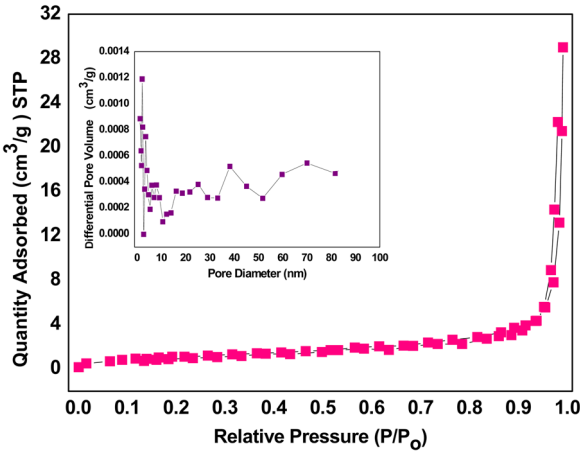

Fig. 3 Nitrogen sorption isotherm of m-FeCTB nanomaterial.

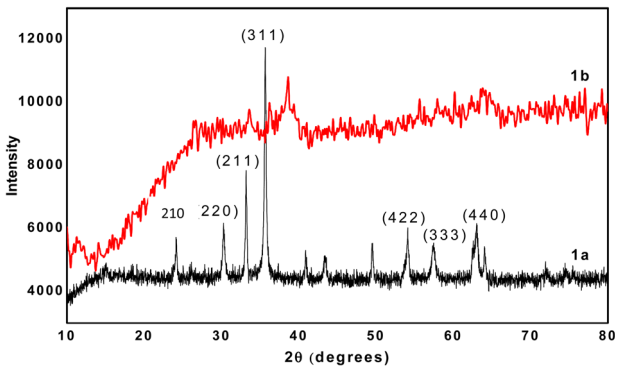

Fig. 4 Wide-angle PXRD patterns of (a) calcined and (b) uncalcined m-FeCTB.

The remaining peaks might be due to some impurities like bromide at 42° and FeO at 49°.

Fe 2p peaks at ~709 eV and 724 eV, a C 1s peak at 285.0 eV, and an O 1s peak at 530.5 eV are visible in the XPS survey spectrum (Fig. 5a) and the high-resolution spectra for Fe 2p, O 1s, and C 1s (Fig. 5b–d). The results provide evidence that the template was successfully incorporated into the Fe nanomaterial. The peak in the high-resolution O 1s spectrum at 530.5 eV corresponds to the typical binding energy for Fe–O bonding. The value of 531 eV found in the O 1s spectrum matches γ-Fe_2O_3's predicted value quite well.[11,29] Additionally, substantial molecular carbon is found in the iron nanomaterial (Fig. 6d). The peak at binding energy of 284.8 eV is attributed to the C–C bond. Although adventitious carbon contamination is likely to occur during the chemical process, our results indicate that the product is a mixture of Fe_2O_3 and FeO, and we can consider m-FeCTB as an iron nanocomposite.

The surface acidity of the FeCTB nanomaterial was measured using ammonia temperature programmed desorption (NH_3-TPD) (Fig. S2, ESI†), and the total acidity was calculated to be 26 μmol g^{-1}. The NH_3-TPD profile of FeCTB showed two peaks at 189 °C and at 325 °C, which can be ascribed to Lewis acid sites due to the presence of the Fe_2O_3 phase. The weaker acid strength of the calcined FeCTB provides significant improvement in selectivity for glucose and HMF.

The H_2-TPR profile (Fig. S3, ESI†) confirms that the iron nanomaterial has active site Fe^{2+} species in the form of FeO and Fe_3O_4. The XPS results (Fig. 5) also favor the presence of Fe^{2+} species as the active species for cellobiose hydrolysis.

VSM analysis was performed by determining the magnetic field dependence of magnetization (MH curve). The hysteresis loop of the iron nanomaterial at 300 K shown in Fig. 6 confirms the ferromagnetic nature with a magnetic saturation value of 32 emu g^{-1}. The ferromagnetic nature of the iron nanomaterial makes it a magnetically recoverable, cost-effective, and environmentally friendly catalyst. Coercivity (61 Oe) is inversely proportional to the particle size and hence is in agreement with the particle size determined using TEM.

Table 1 describes the physicochemical properties of various catalysts employed in the hydrolysis of cellobiose. The synthesized m-FeCTB catalyst has a surface area of 30 m^2 g^{-1}, particle size of 60 nm from TEM analysis and 120 nm (Fig. S1, ESI†) from DLS with ~15% iron content and a magnetic saturation value of 32 emu g^{-1}, as shown in Table 1. The recently reported catalyst mesoporous carbon-Fe_2O_3γ-Fe_2O_3 has surface area of 17 m^2 g^{-1}, which is almost the same as our synthesized catalyst, and low iron content (12%) with a small particle size of 10 nm.[27] The synthesized m-FeCTB catalyst has a very small pore size ranging from 5 to 35 nm, surface area of ~30 m^2 g^{-1} and high crystallinity, which are the most favorable parameters for hydrolysis reaction.

3.2 Experimental setup for determination of catalytic activity (hydrolysis reaction)

A 30-mL glass reactor (closed vessel) was used to study the hydrolysis of cellobiose in aqueous phase. The catalytic activity was investigated using the following conditions: catalyst 0.2 mg, 0.5 mg of cellobiose, 25 mL of water, reaction temperature of 120 °C, and reaction time 6 h at atmospheric pressure. The hydrolysis reaction within the glass setup was initiated by placing it in a preheated oil bath. Negligible cellobiose conversion (9%) was obtained after 6 h of reaction time under these conditions in the absence of the m-FeCTB catalyst (blank test). The carbon balance, determined by the concentration of all products analyzed using HPLC, was nearly 100% during the entire experiment.

3.3 Catalytic activity

Cellobiose was depolymerized to fine chemicals using hydrolysis using the magnetically separable m-FeCTB nanomaterial as a catalyst. Table 2 shows the overall conversion and product yield. The yield of the products and the hydrolysis rate were calculated based on the UV spectroscopy data. The UV-visible results (Fig. S4, ESI†) confirm the presence of glucose at 271 nm with an absorbance of 1.27 and HMF at 210 nm with an absorbance of 0.58. The catalytic activity of cellobiose hydrolysis was determined by measuring the absorbance at 284 nm for cellobiose. The products obtained were glucose and HMF.

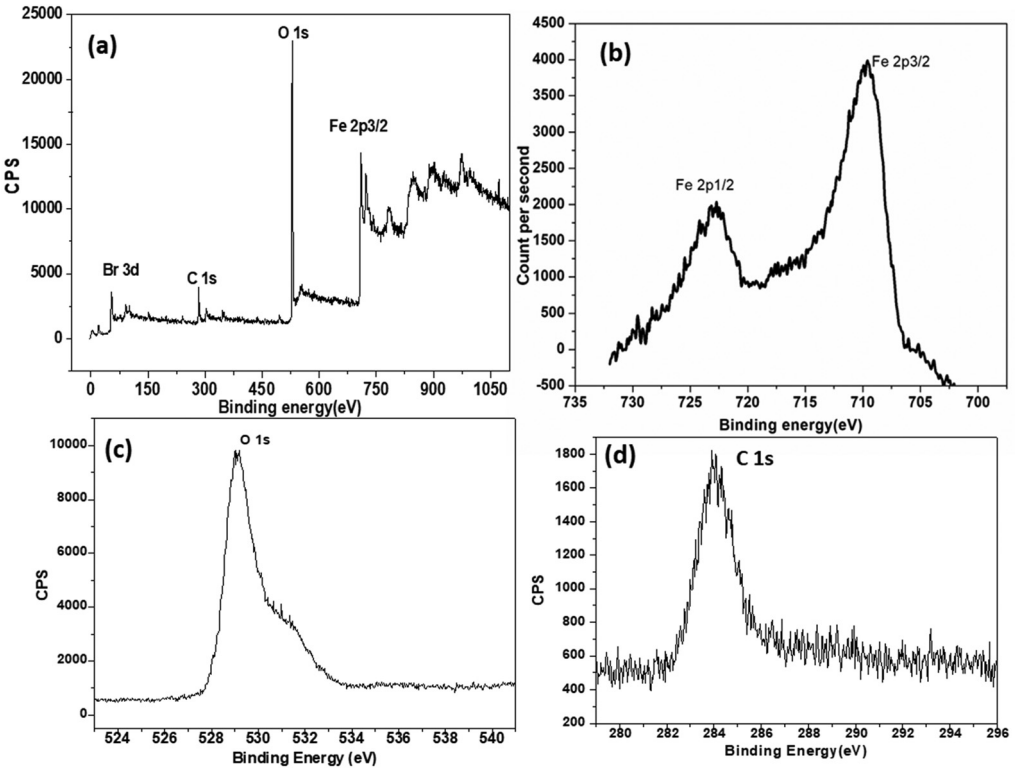

Fig. 5 (a) XPS survey spectrum, (b) high-resolution Fe 2p spectrum, (c) high-resolution O 1s spectrum, and (d) high-resolution C 1s spectrum for FeCTB nanomaterial.

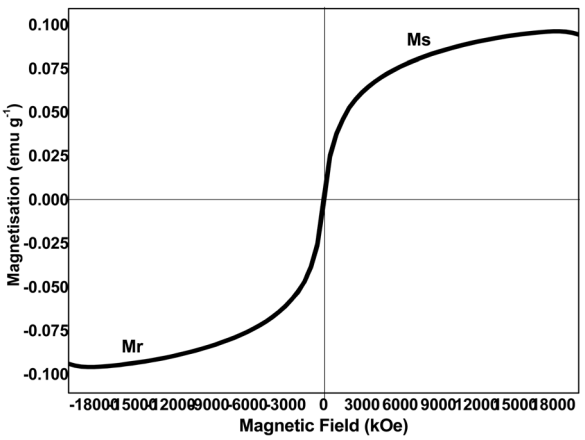

Fig. 6 VSM graph of iron nanomaterial (m-FeCTB catalyst).

This material showed comparable hydrolysis activity at 120 °C for 6 h yielding glucose and HMF as the major products. The identification of hydrolyzed products was done using HPLC. The HPLC results show 80% cellobiose conversion and the presence of glucose and HMF as the hydrolyzed products (Fig. 7). The yield of glucose was calculated to be 60%, and the yield of HMF was 40% using glucose and cellobiose as external standards with hydrolysis by m-FeCTB at 120 °C. The peak at 19.9 min might be due to impurities stuck in the HPLC column, and this peak is clearly shown in all the chromatograms.

The hydrolysis activity of mesoporous m-FeCTB might be due to the high surface area, small particle size, high porosity, crystallinity, mild Lewis acidity (Fe^{2+}), and presence of the γ-Fe_2O_3 phase in the catalyst. It was reported that in acidic conditions, cellobiose is hydrolyzed to glucose, which can then be isomerized and dehydrated to produce HMF.[28,30,31] During the hydrolysis reaction, impurities present in the FeCTB nanomaterial, such as iron salt ($FeCl_3$ and FeO), might act as Lewis acids and *in situ* generation of Brønsted acids in aqueous medium could enhance the hydrolysis of the β-1,4-glycosidic bonds of cellobiose.[31,32] The first step for disaccharide (cellobiose) hydrolysis is adsorption on the iron surface. Therefore,

Table 1 Physicochemical properties of iron-based catalysts

Catalyst	Surface area ($m^2\ g^{-1}$)	Pore size (BJH) (nm)	Magnetic nature	Particle size (nm)	Metal (weight%)	Acidity (μmol $NH_3\ g^{-1}$)
m-FeCTB	30	35	Ferromagnetic nature magnetic saturation (Ms) = 32 emu g^{-1}	45–60	15	26
Mesoporous carbon-$Fe_2O_{3-\gamma}$ Fe_2O_3[27]	17	40	Magnetic saturation (Ms) −8.4 emu g^{-1}	5–10	12	—

Table 2 Comparative study of nanomaterials (catalysts) used for the hydrolysis of cellulose and cellobiose

Catalyst	Conversion (%)	Reaction conditions	Product yield and distribution
m-FeCTB	80	T = 120 °C, water, feed:catalyst = 1 : 1, reaction time = 6 h	Glucose (40%), HMF (60%)
m-FeCTB	85	T = 250 °C, water, feed:catalyst = 1 : 1, reaction time = 6 h	Glucose (30%), HMF (70%)
Mesoporous carbon-$Fe_2O_3\gamma$ Fe_2O_3[28]	(Glucose formation) 85	T = 120 °C, water, feed:catalyst = 1 : 1, reaction time = 6 h	Glucose (85% yield), levulinic acid, HMF,
Mesoporous activated carbon (SAS)[26]	60	500 mg of cellulose, 125 mg of catalyst, 25 mL of water, T = 190 °C, reaction time = 3 h	Glucose (52%), HMF (22%), others (26%)
TiO_2-based catalyst[30]	90	4 g of cellobiose, 2 g of catalyst, 80 mL of water, T = 140 °C, time = 6 h	Glucose (73%), HMF (14%)
Iron(III)[27]	79	Cellulose, 0.10 g; catalyst, 0.00287 mol dm^{-3} (0.00144 mol dm^{-3} $Fe_2(SO_4)_3$); H_2SO_4, 2 wt%; H_2O, 6 cm^3; O_2, 30 bar; temperature, 160 °C; time, 2 h	Formic acid (45%)
H-[Al]-magadiite[32]	80	Cellobiose at 0.03 mol g^{-1}, 0.2 g of catalyst, T = 140–180 °C, time = 7 h	Glucose (45%), HMF (16%), fructose (9%)

the higher the number of adsorption sites, the higher the chance of achieving larger conversion of cellobiose. Cellobiose hydrolysis and glucose production depend on Brønsted acid sites.[32]

The catalyst is completely recoverable from the reaction medium, thus minimizing the environmental impact of any industrial process where it would be employed. A recent report showed 50% higher hydrolysis activity of FeCTB catalysts (containing γ-Fe_2O_3) compared to conventional catalysts.[28] Research was conducted by Shen and Wyman to produce levulinic acid from cellulose as the major product using hydrochloric acid as the catalyst.[26] The reported yield of levulinic acid was ~60%.[26] In spite of the desirable results obtained from homogenous catalysts, the development of solid acid catalysts is urgently demanded. Heterogeneous catalysts offer various advantages, including being economically feasible, easily recoverable, and environmentally friendly.[26,28–31]

Table 2 summarizes the comparative hydrolysis study of cellobiose using different catalysts. The most frequently used solid acid catalyst is Amberlyst 70, compared with HCl, which has lower selectivity for cellobiose hydrolysis and its conversion into HMF and formic acid.[26,28] Hydrolysis of cellobiose over TiO_2-based catalyst (Ti-W600) in aqueous phase yielded glucose (73%) and HMF (14%). The activity and selectivity for glucose depend on the dopant (W or Zr), calcination temperature and

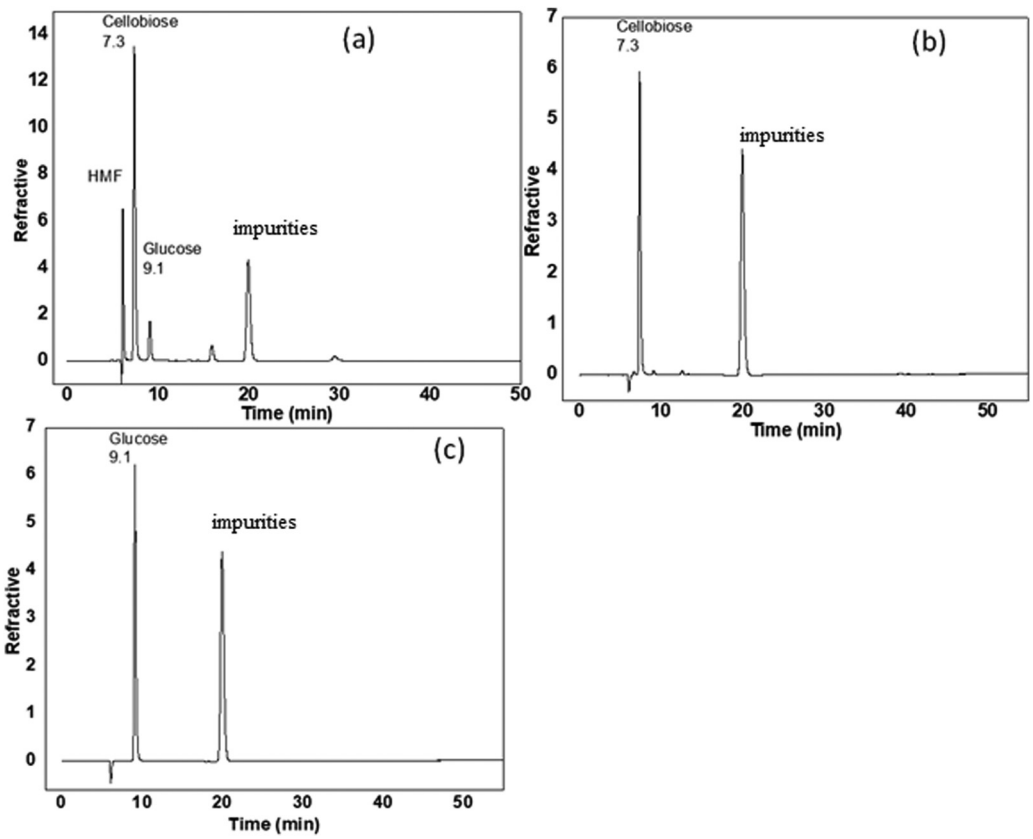

Fig. 7 HPLC analysis of (a) hydrolyzed cellobiose products, (b) aqueous cellobiose standard, and (c) glucose standard.

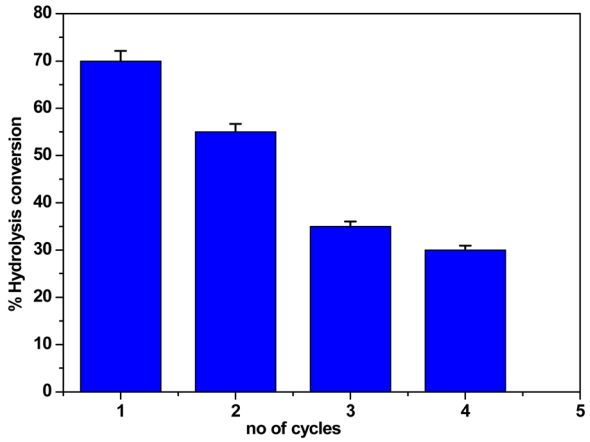

Fig. 8 Recyclability of m-FeCTB nanomaterial for cellobiose hydrolysis at 120 °C.

due to promising solid acid catalyst.[30] Cellobiose hydrolysis over m-FeCTB nanomaterial at 120 °C achieved 80% conversion with 60% HMF yield and 40% glucose yield (Table 2, row 1), whereas only 8% was hydrolyzed by hydrochloric acid under the same conditions. The m-FeCTB catalyst under moderate reaction conditions achieved better cellobiose hydrolysis activity, with a turnover frequency (TOF) of 0.037 s^{-1}, compared to the reported Amberlyst 70 and iron(III)[27] catalysts (Table 1).

Table S1 (ESI†) shows the results of experiments comparing different iron nanomaterials synthesized using the same method with different calcination temperatures. The hydrolysis conversion increased from 50% to 80%, and the yield of glucose increased from 50 to 60% over the iron nanomaterial with increasing calcination temperature from 200 to 300 °C. At 400 °C calcination temperature, the maximum conversion of 80% was achieved with 40% glucose yield and 60% HMF yield. This might be because the calcination temperature greatly influences the crystalline phases and acid property of the catalysts, improving the catalytic activity. Table S2 (ESI†) shows the effect of reaction temperature on the hydrolysis. The slight increase in hydrolysis conversion from 80% to 85% with increasing temperature from 120 to 250 °C (Table S2, ESI†) is due to the thermal effect along with catalytic hydrolysis. The maximum yield of HMF (70%) and glucose (30%) was achieved at 250 °C under the same reaction conditions.

The hydrolysis of cellobiose using the cost-effective, magnetically separable m-FeCTB catalyst in a glass assembly (closed vessel) at low temperature and atmospheric pressure in 6 h is the novel aspect of this study along with the synthesis. The high surface area, ferromagnetic nature, porosity, high crystallinity, presence of γ-Fe_2O_3 and small particle size are the novelty of the m-FeCTB catalyst required for cellobiose hydrolysis.

3.4 Recyclability test

After the first cycle of cellobiose hydrolysis (70% conversion), the m-FeCTB catalyst was recovered and employed. The highest cellobiose conversion (55%) was observed during the second reuse of the catalyst for cellobiose hydrolysis (Fig. 8). Additionally, cellobiose conversion was seen in the third cycle of hydrolysis, at a rate of 35%. However, a substantially lower conversion rate, namely 30%, was recorded during the fourth cycle (Fig. 8). It was concluded that that the loss of acid sites and crystallinity from the surface may cause the decrease in cellobiose conversion.

4 Conclusions

A magnetically separable mesoporous iron nanomaterial catalyst was prepared and tested for the hydrolysis of cellobiose, a model of cellulose. The catalyst was synthesized with iron chloride using CTAB as a template *via* coprecipitation method. The yield of glucose was 40% with a glucose formation rate of 0.65 mg h^{-1} after 6 h of reaction at 120 °C for the hydrolysis of cellobiose using m-FeCTB nanomaterial. The high hydrolysis activity with 80% conversion and TOF of 0.037 s^{-1} at low temperature was attributed due to the small particle size, high porosity (mesoporous), presence of the gamma phase of Fe_2O_3, and mild acidity. This work presents a simple catalytic route for the conversion of cellulose to useful chemicals. This is a new and cost-effective approach for biomass valorization other than the expensive hydrogenation route.

Author contributions

Dr Hari Singh: conceptualization, writing – original draft preparation, visualization, and investigation. Dr Anil Kumar Sinha: idea conceived, reviewing and editing, and research execution. Dr Sharanmeet Kour: experiments and sample collection. Dr Gaurav Goel: software, data interpretation, and editing. Prof. Suneel Singh Berhyan: characterization, interpretation and sample records, and editing. Dr J Mishra: proofreading, editing, and grammar correction.

Declaration statement

We confirm that the paper has been read, reviewed, and approved by all the indicated authors and that no other people who are eligible to be an author but are not listed have worked on the project. We further reiterate that the order in which the authors are listed in the manuscript is one that we all agreed upon. We certify that we have taken all necessary precautions to preserve the intellectual property connected to this work and that there are no intellectual property-related barriers to publication.

Conflicts of interest

All the authors declare that they have no competing interests.

Acknowledgements

HS acknowledges the support from the Department of Chemistry, RIMT University Mandi Gobindgarh, Punjab and CSIR-IIP Dehradun, AcSIR, and AMU Aligarh.

References

1 C. H. Zho, X. Xia, C. X. Lin, D. S. Tong and J. Beltramini, Catalytic conversion of lignocellulosic biomass to fine chemicals and fuels, *Chem. Soc. Rev.*, 2011, **40**, 5588–5617.
2 N. Akhtar, K. Gupta, D. Goyal and A. Goyal, Recent advances in pretreatment technologies for efficient hydrolysis of lignocellulosic biomass, *Environ. Prog. Sustainable Energy*, 2016, **35**, 489–511.
3 T. K. Ghose, P. V. Pannir Selvam and P. Ghosh, Catalytic solvent delignification of agricultural residues: organic catalysts, *Biotechnol. Bioeng.*, 1983, **25**, 2577–2590.
4 Y. Sun and J. Cheng, Hydrolysis of lignocellulosic materials for ethanol production: a review, *Bioresour. Technol.*, 2002, **83**, 1–11.
5 H. Chen, J. Liu, X. Chang, D. Chen, Y. Xue and P. Liu, A review on the pretreatment of lignocellulose for high-value chemicals, *Fuel Process. Technol.*, 2017, **160**, 196–206.
6 M. E. Himmel, S. Y. Ding, D. K. Johnson, W. S. Adney, M. R. Nimlos and J. W. Brady, Biomass recalcitrance: engineering plants and enzymes for biofuels production, *Science*, 2007, **315**, 804–807.
7 W. Farhat, R. A. Venditti, M. Hubbe, M. Taha, F. Becquart and A. Ayoub, A review of water-resistant hemicellulose-based materials: processing and applications, *ChemSusChem*, 2017, **10**, 305–323.
8 P. Duarah, D. Haldar and M. K. Purkait, Technological advancement in the synthesis and applications of lignin-based nanoparticles derived from agro-industrial waste residues: a review, *Int. J. Biol. Macromol.*, 2020, **163C**, 1828–1843.
9 D. Haldar, D. Sen and K. Gayen, A review on the production of fermentable sugars from lignocellulosic biomass through conventional and enzymatic route-a comparison, *Int. J. Green Energy.*, 2016, **13**, 1232–1253.
10 C. E. Araújo Padilha, C. da Costa Nogueira, M. A. Oliveira Filho, F. C. de Sousa Júnior, C. F. de Assis, D. F. de Santana Souza, J. A. de Oliveira and E. S. dos Santos, Fractionation of green coconut fiber using sequential hydrothermal/alkaline pretreatments and Amberlite XAD-7HP resin AD-7HP resin, *J. Environ. Chem. Eng.*, 2019, **7**, 103474.
11 R. Rai, M. Bibra, B. S. Chadhs and R. K. Saini, Enhanced hydrolysis of lignocellulosic biomass with doping of a highly thermostable recombinant laccase, *Int. J. Biol. Macromol.*, 2019, **137**, 232–237.
12 M. F. Mustafa, Y. Liu, Z. Duan, H. Guo, S. Xu, H. Wang and W. Lu, Volatile compounds emission and health risk assessment during composting of organic fraction of municipal solid waste, *J. Hazard. Mater.*, 2016, **327**, 35–43.
13 Z. Usmani, M. Sharma, Y. Karpichev, A. Pandey, R. C. Kuhad, R. Bhat, R. Punia, M. Aghbashlo, M. Tabatabaei and V. K. Gupta, Advancement in valorization technologies to improve utilization of bio-based waste in bio economy context, *Renewable Sustainable Energy Rev.*, 2020, **131**, 1321–1364.
14 X. Liu, R. Bayard, H. Benbelkacem, P. Buffiere and R. Gourdon, Evaluation of the correlations between biodegradability of lignocellulosic feedstocks in the anaerobic digestion process and their biochemical characteristics, *Biomass Bioenergy*, 2015, **81**, 534–543.
15 F. Tufaner and Y. Avsar, Effects of co-substrate on biogas production from cattle manure: a review, *Int. J. Environ. Sci. Technol.*, 2016, **13**, 2303–2312.
16 S. Luo, Y. Zhou and C. Yi, Syngas production by catalytic steam gasification of municipal solid waste in a fixed-bed reactor, *Energy*, 2012, **44**, 391–395.
17 B. Kumar and P. Verma, Techno-economic assessment of biomass-based integrated biorefinery for energy and value-added product, in *Biorefineries: a step towards renewable and clean energy*, Clean energy production technologies, Springer, 2021, pp. 581–616.
18 F. Meneguzzo, C. Brunetti, A. Fidalgo, R. Ciriminna, R. Delisi, L. Albanese, F. Zabini, A. Gori, L. B. dos Santos Nascimento, A. De Carlo, F. Ferrini, L. M. Ilharco and M. Pagliaro, Real-scale integral valorization of waste orange peel *via* hydrodynamic cavitation, *Processes*, 2019, **7**, 581.
19 H. C. Ong, W. H. Chem, A. Farooq, Y. Y. Gan, K. T. Lee and V. Ashokkumar, Catalytic thermochemical conversion of biomass for biofuel production: a comprehensive review, *Renewable Sustainable Energy Rev.*, 2019, **113**, 109266.
20 S. Y. Foong, Y. H. Chan, W. Y. Cheah, N. H. Kamaludin, T. Ibrahim, C. Sonne, W. Peng, P. L. Show and S. S. Lam, Progress in waste valorization using advanced pyrolysis techniques for hydrogen and gaseous fuel production, *Bioresour. Technol.*, 2020, **S0960–8524**, 31573.
21 O. A. Fakayode, E. A. A. Aboagarib, C. Zhou and H. Ma, Co-pyrolysis of lignocellulosic and macroalgae biomasses for the production of biochar-A review, *Bioresour. Technol.*, 2020, **297**, 122–408.
22 S. Kim and M. T. Holtzapple, Lime pretreatment and enzymatic hydrolysis of corn stover, *Bioresour. Technol.*, 2005, **96**, 1994–2006.
23 M. Marzo, A. Gervasini and P. Carniti, Hydrolysis of disaccharides over solid acid catalysts under green conditions, *Carbohydr. Res.*, 2012, **347**, 23–31.
24 L. Vilcocq, P. C. Castilho, F. Carvalheiro and L. C. Duarte, Hydrolysis of oligosaccharide over solid acid catalysts, *ChemSusChem*, 2014, **7**, 1010–1019.
25 H. Singh, A. Rai, R. Yadav and A. K. Sinha, Glucose hydrogenation to sorbitol over unsupported mesoporous Ni/NiO catalyst, Molecular, *Catalysis*, 2018, **451**, 186–191.
26 F. Z. Azar, M. A. Lillo Ródenas and M. C. Román, Martínez, Cellulose hydrolysis is catalyzed by mesoporous activated carbons functionalized under mild conditions, *SN Appl. Sci.*, 2019, **1**, 1739.
27 Y. Hou, Z. Lin, M. Niu, S. Ren and W. Wu, Conversion of cellulose into formic acid by iron(III)-catalyzed oxidation with O_2 in acidic aqueous solutions, *ACS Omega*, 2018, **3**, 14910–14917.
28 D. Yamaguchi, K. Watenabe and S. Fukumi, Hydrolysis of cellulose by a mesoporous carbon-$Fe_2(SO_4)_3$/γ-Fe_2O_3 nanoparticle-based solid acid catalysts, *Sci. Rep.*, 2016, **6**, 20327.

29 T. Ennaert, S. Feys, D. Hendrikx, P. A. Jacobs and B. F. Sels, Reductive splitting of hemicellulose with stable ruthenium-loaded USY zeolites, *Green Chem.*, 2016, **18**, 5295–5304.
30 L. Vilcocq, E. DouardRebmann, Y. Wayne Cheah and P. Fongarland, Hydrolysis of cellobiose and xylan over TiO2 based catalysts, *ACS Sustainable Chem. Eng.*, 2018, **6**, 5555–5565.
31 G. S. Foo, A. H. Van Pelt, D. Krötschel, B. F. Sauk, A. K. Rogers, C. R. Jolly, M. M. Yung and C. Sievers, Hydrolysis of cellobiose over selective and stable sulfonated activated carbon catalysts, *ACS Sustainable Chem. Eng.*, 2015, **3**, 1934–1942.
32 G. P. Campos, E. M. Albuquerque, M. A. Fraga and H. O. Pastore, Continuous cellobiose hydrolysis over lamellar aluminosilicates-unveiling [Al]-magadiite water-tolerant acid sites, *Ind. Eng. Chem. Res.*, 2021, **60**, 4794–4805.